

Super-Nyquist asteroseismology of solar-like oscillators with *Kepler* and K2—expanding the asteroseismic cohort at the base of the red-giant branch

W. J. Chaplin^{1,2*}, Y. Elsworth^{1,2}, G. R. Davies^{1,2}, T. L. Campante^{1,2}, R. Handberg^{1,2}, A. Miglio^{1,2} and S. Basu³

¹ School of Physics & Astronomy, University of Birmingham, Edgbaston, Birmingham, B15 2TT, UK

² Stellar Astrophysics Centre (SAC), Department of Physics and Astronomy, Aarhus University, Ny Munkegade 120, DK-8000 Aarhus C, Denmark

³ Department of Physics and Astronomy, Yale University, P.O. Box 208101, New Haven, CT, 06520, USA

10 July 2018

ABSTRACT

We consider the prospects for detecting solar-like oscillations in the “super-Nyquist” regime of long-cadence (LC) *Kepler* photometry, i.e., above the associated Nyquist frequency of $\approx 283 \mu\text{Hz}$. Targets of interest are cool, evolved subgiants and stars lying at the base of the red-giant branch. These stars would ordinarily be studied using the short-cadence (SC) data, since the associated SC Nyquist frequency lies well above the frequencies of the detectable oscillations. However, the number of available SC target slots is quite limited. This imposes a severe restriction on the size of the ensemble available for SC asteroseismic study. We find that archival *Kepler* LC data from the nominal Mission may be utilized for asteroseismic studies of targets whose dominant oscillation frequencies lie as high as $\approx 500 \mu\text{Hz}$, i.e., about 1.75-times the LC Nyquist frequency. The frequency detection threshold for the shorter-duration science campaigns of the re-purposed *Kepler* Mission, K2, is lower. The maximum threshold will probably lie somewhere between ≈ 400 and $450 \mu\text{Hz}$. The potential to exploit the archival *Kepler* and K2 LC data in this manner opens the door to increasing significantly the number of subgiant and low-luminosity red-giant targets amenable to asteroseismic analysis, overcoming target limitations imposed by the small number of SC slots. We estimate that around 400 such targets are now available for study in the *Kepler* LC archive. That number could potentially be a lot higher for K2, since there will be a new target list for each of its campaigns.

Key words:

asteroseismology – methods: data analysis – stars: oscillations

1 INTRODUCTION

The NASA *Kepler* Mission has provided photometric observations of exquisite quality for asteroseismic studies of a diverse range of pulsating stars (Gilliland et al. 2010). Particularly noteworthy has been the large volume of data collected on cool main-sequence, subgiant and red-giant stars showing solar-like oscillations, pulsations that are excited and intrinsically damped by near-surface convection (Chaplin & Miglio 2013). The successful asteroseismology programme looks set to continue in the re-purposed *Kepler* Mission, K2 (Howell et al. 2014). The quality of the K2 photometry for asteroseismic studies of coherent pulsators has already been demonstrated by results from engineering test data (Jeffery & Ramsay 2014; Hermes et al. 2014). The photometric performance has

also confirmed the predicted potential for studies of solar-like oscillators (Chaplin et al. 2013), studies that will be made possible by the longer, full-campaign science data.

Kepler data were collected in two cadences (Koch et al. 2010) during the 4-yr-long nominal Mission. Data on up to 170,000 targets were available in the 29.4-minute long cadence (LC), whilst a much smaller total of up to 512 targets could be observed simultaneously in the 58.85-second short cadence (SC). These cadences establish Nyquist frequencies for the two modes of operation of $\approx 283 \mu\text{Hz}$ (in LC) and $\approx 8496 \mu\text{Hz}$ (in SC). The LC Nyquist frequency coincides with the dominant periods of oscillation shown by cool stars that lie just above the base of the red-giant branch. Both cadences have been maintained for the K2 Mission, but the total number of targets for each observing campaign has been reduced – to approximately 10,000 and 50 targets, respectively – because of the need for larger pixel target masks.

The detection of solar-like oscillations in cool main-sequence

* E-mail: w.j.chaplin@bham.ac.uk

and subgiant stars, and stars at the very bottom of the red-giant branch, demands that the target-limited SC data be utilized since the dominant periods of oscillation are shorter than one hour. Observations made in the numerous long-cadence slots are sufficient to detect oscillations in more evolved red giants, because the relevant pulsation periods are longer.

Oscillations have already been detected in around 16,000 red giants in the nominal Mission LC data (Hekker et al. 2011; Stello et al. 2013; Huber et al. 2014). Whilst *Kepler* increased the number of cool main-sequence and subgiant stars with asteroseismic data by over an order of magnitude, to around 700 targets (Chaplin et al., 2011a, 2014; Huber et al. 2013), totals were nevertheless limited by the available number of SC target slots. The possibility of detecting solar-like oscillations in LC data *above* the LC Nyquist frequency – i.e., in the “super-Nyquist” regime – offers the potential to increase significantly the number of evolved subgiant and low-luminosity red-giant targets amenable to asteroseismic study.

The use of LC data for super-Nyquist studies of coherent pulsators has been considered in some detail by Murphy et al. (2013). Baran et al. (2012) also employed a super-Nyquist analysis of a compact pulsator observed in SC. While Gaulme et al. (2013) and Beck et al. (2014) identified a few red giants with oscillation frequencies above the LC Nyquist frequency, the prospects for studying solar-like oscillators in the LC super-Nyquist regime have not yet been explored in any detail. Our aim in this paper is to consider the utility of the archival *Kepler* and future K2 data for such studies.

The layout of the rest of the paper is as follows. We begin in Section 2 with a summary of some of the basic principles from Fourier analysis that are relevant to our study. We then consider in Section 3 the specific case of *Kepler* long-cadence observations; and in Section 4 we go on to consider the characteristics of the super-Nyquist spectrum shown by solar-like oscillators, considering the impact of the finite mode lifetimes (Section 4.1), the use of a priori information to discriminate true from aliased peaks in the frequency spectrum (Section 4.2), and the reduced S/N above the Nyquist frequency (Section 4.3). We include model predictions for subgiant and low-luminosity red giant stars, and real super-Nyquist examples from the *Kepler* archive (Section 4.4). We finish the paper in Section 5 with concluding remarks.

2 BASIC PRINCIPLES

Let us begin by considering the simple case of a sinusoidal signal of frequency ν , sampled at regular intervals Δt in time. This establishes a sampling frequency $\nu_s = (\Delta t)^{-1}$. The well-known sampling theorem (Nyquist 1928; Shannon 1949) tells us that when $\nu \leq \nu_s/2$, the sampling is sufficient to completely determine the signal – we say the signal is oversampled – and there is no ambiguity in the measured frequency. We may also write the sampling requirement as $\nu \leq \nu_{\text{Nyq}}$, where the Nyquist frequency, ν_{Nyq} , is defined as

$$\nu_{\text{Nyq}} \stackrel{\text{def}}{=} \nu_s/2 \equiv (\Delta t)^{-1}. \quad (1)$$

What happens if instead the signal is undersampled, so that $\nu > \nu_{\text{Nyq}}$? Power will be present in the “super-Nyquist” regime of the frequency spectrum at the true frequency, ν ; and it will also now be reflected, or aliased, back into the frequency region below ν_{Nyq} . If we write the true frequency as $\nu = \nu_{\text{Nyq}} + \nu'$, there will be peaks at $\nu_{\text{Nyq}} + \nu'$ and $\nu_{\text{Nyq}} - \nu'$. There is now an ambiguity in the estimated frequency, and we are completely reliant on using other knowledge to pick the true frequency. We shall see that irregular time sampling

offers the potential to lift this degeneracy provided the signal is coherent, or nearly coherent, over the duration of the observations (of which more in Section 3 below).

The appearance of the frequency spectrum is also affected by the amount of time during each cadence Δt that is used to collect data, i.e., in our case, to integrate photons from the target star. If a high fraction of each cadence is used to collect data, we may significantly underestimate the true amplitude because each datum may average the time-varying signal. If the integration time per cadence is $\Delta t'$, then a signal of frequency ν will have its amplitude attenuated by the factor (e.g., Campante 2012):

$$\eta = \text{sinc} [\pi (\nu \Delta t')]. \quad (2)$$

When the fraction of each cadence given over to integration is unity, so that $\Delta t' = \Delta t$, the attenuation may then be written as (e.g., Chaplin et al. 2011b; Huber et al. 2011; Murphy 2012):

$$\begin{aligned} \eta &= \text{sinc} [\pi (\nu \Delta t)] = \text{sinc} \left[\pi \left(\frac{\nu}{\nu_s} \right) \right] \\ &\equiv \text{sinc} \left[\pi/2 \left(\frac{\nu}{\nu_{\text{Nyq}}} \right) \right]. \end{aligned} \quad (3)$$

The attenuation in power is given by the square of the sinc function, η^2 . Even when the integration duty cycle is close to 100 per cent and the attenuation is at its strongest – which is the case for *Kepler*; see Section 3 below – Equation 3 indicates that one still has sensitivity to signals in the super-Nyquist regime ($\nu > \nu_{\text{Nyq}}$) since the first zero of the sinc function does not occur until $\nu = \nu_s \equiv 2\nu_{\text{Nyq}}$. It is also worth remarking that even when signals are oversampled, so that $\nu \leq \nu_{\text{Nyq}}$, there is still significant attenuation close to the Nyquist frequency.

3 KEPLER LONG-CADENCE OBSERVATIONS

The *Kepler* LC data are comprised of $\Delta t = 29.4$ -min cadences (Jenkins et al. 2010) that are exactly regular in the spacecraft frame of reference. This establishes a notional LC Nyquist frequency of $\nu_{\text{Nyq}} \approx 283 \mu\text{Hz}$. Each 29.4-min cadence is in turn a summation of 270 individual ≈ 6 -sec readouts (e.g., Gilliland et al. 2011). Most of each cadence is therefore given over to the collection of photons. The very high fractional duty cycle for the *Kepler* integrations means the signal attenuation follows closely that described by Equation 3.

The left-hand panel of Fig. 1 shows the frequency-power spectrum of idealized observations, made on a regular *Kepler*-like cadence, of several undersampled sinusoids. The sinusoids are all of unit amplitude and have frequencies lying in the super-Nyquist regime between $310 \mu\text{Hz}$ and $460 \mu\text{Hz}$. Peaks due to the true frequencies are rendered as black lines. The vertical dashed lines mark multiples of ν_{Nyq} . Peaks in grey are therefore aliases of the true frequencies. The spectrum is repeated every $2\nu_{\text{Nyq}}$ because of the discrete nature of the calculation.

This power spectrum has been calibrated¹ so that a sinusoid of unit amplitude with an infinite sample rate would show a maximum power per bin of unity. The observed powers at the true frequencies are much lower than unity, the true power. This is due to the

¹ Here, and throughout the rest of the paper, we show spectra calibrated in power per bin or power per Hz – as opposed to amplitude per root bin or per root Hz – since this is the usual approach when analysing solar-like oscillators (which we will come to later in Section 4 below).

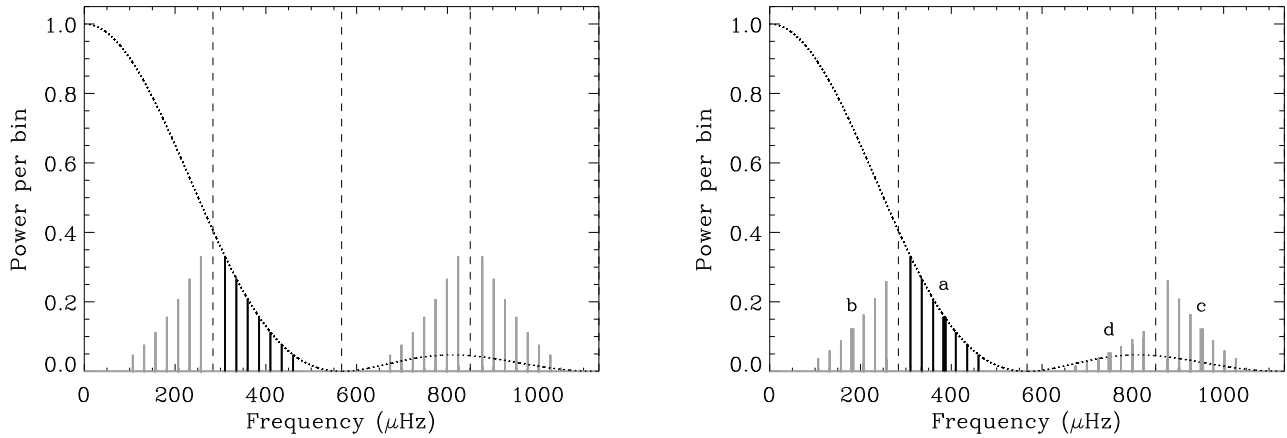


Figure 1. Left-hand panel: Frequency-power spectrum for a series of sinusoids of unit amplitude having frequencies between $310 \mu\text{Hz}$ and $460 \mu\text{Hz}$, sampled on a regular cadence. Peaks due to the true frequencies are rendered as black lines. The vertical dashed lines mark multiples of ν_{Nyq} . Peaks in grey are aliases of the true frequencies. The dotted line marks the sinc-squared attenuation envelope (i.e., η^2). Right-hand panel: Spectrum now given by irregular sampling of the undersampled sinusoids. The true peak and the aliases of one of the frequencies are rendered in thick linestyles (see text).

sinc-function attenuation described by Equation 3. The dotted line marks the sinc-squared suppression envelope in power, i.e., η^2 .

The above is not quite the whole story as far as timing issues for the *Kepler* observations are concerned. *Kepler* lies in a 372.5-day heliocentric, Earth-trailing orbit. Observations of the pulsations of a *Kepler* target – be it one in the original field, or in the K2 fields in the ecliptic plane – will be phase modulated in the spacecraft frame of reference. This is because there is a component of the orbital motion of *Kepler* along the line-of-sight (target) direction, which delays or advances the arrival time of light from the star. The annual size of the effect is approximately ± 190 sec for targets in the original field, and approximately ± 500 sec for targets in the ecliptic (where the K2 fields lie).

To compensate for this effect² the *Kepler* time stamps are corrected to Barycentric arrival times (actually Barycentric Dynamical Time; see, e.g., García et al. 2014). An important consequence is that the intervals between time stamps are no longer regular, but are modulated periodically on a ~ 1 -yr timescale. This periodic modulation splits the aliased peaks in the frequency spectrum into many components, as discussed in detail by Murphy et al. (2013).

The right-hand panel of Fig. 1 shows the result of simulating LC observations of an idealized star in the original *Kepler* field undergoing coherent pulsations. The artificial data span four simulated years and include the aforementioned timing effects. The simulated pulsations are the same, undersampled sinusoids from the left-hand panel. Notice how the aliases are no longer exact, reflected copies about multiples of ν_{Nyq} . Some copies have different maximum power spectral densities (i.e., peak heights in the spectrum) than others. The reason for this is that the splitting of the power into several components reduces the maximum heights in Fig. 1, relative to those expected for simple reflected aliases (the total integrated power in the aliases is conserved).

The top left-hand panel of Fig. 2 shows a zoom of the peak

due to the true frequency marked ‘a’ in the right-hand panel of Fig. 1, whilst the other panels show zooms its aliases marked ‘b’, ‘c’ and ‘d’ on Fig. 1. As explained by Murphy et al. (2013), the exact manner in which the alias peaks are affected by the timing modulation depends on the relation of their frequencies to the sampling frequency. If the true frequency is ν , then aliases at $n\nu_s \pm \nu$, or equivalently $2m\nu_{\text{Nyq}} \pm \nu$, will share the same structure, e.g., what is predominantly a triplet structure when $n = 1$, or a quintuplet structure when $n = 2$, with the frequency splitting between adjacent components being $\sim 1 \text{ yr}^{-1}$.

Murphy et al. (2013) pointed out that for high-amplitude, coherent pulsations the introduction of sideband structure, which is well resolved in the nominal Mission *Kepler* data, allows one to discriminate the real and aliased peaks. What about solar-like oscillations, which are not coherent and typically have much lower amplitudes (and hence lower S/N levels in the frequency spectrum) than coherent pulsations?

4 SUPER-NYQUIST SPECTRUM OF SOLAR-LIKE OSCILLATIONS

4.1 Impact of finite mode lifetimes

The first issue we confront is that solar-like oscillations have finite lifetimes. In most cases the lifetimes τ of detectable oscillations are significantly shorter than the duration T of the observations (e.g., Dupret et al. 2009). Only for some gravity-dominated mixed modes of red giants do the lifetimes of detected oscillations approach or exceed lengths commensurate with multi-month-long observations. One might therefore not usually expect to be able to resolve the aforementioned sideband structure in the frequency domain.

The underlying noise-free or “limit-spectrum” profiles due to solar-like oscillations are to good approximation Lorentzian in shape, with the FWHM of the peaks given by $\Gamma = (\pi\tau)^{-1}$ (e.g., see Chaplin et al. 2002). Fig. 3 shows how a finite mode lifetime would affect the appearance of the aliased quintuplet from the bottom left-hand panel of Fig. 2. The different linestyles show the composite, aliased limit-spectrum profiles expected when the real mode has a lifetime (linewidth) of 73 days ($0.1 \mu\text{Hz}$; dashed line), 123 days

² Aside from the varying component due to the orbital motion of the spacecraft about the Sun, we assume that there are no other line-of-sight components showing significant variation on the timescale of the observations, e.g., variations due to the target being in a short-period binary (see Davies et al. (2014) for discussion on issues relating to the line-of-sight component).

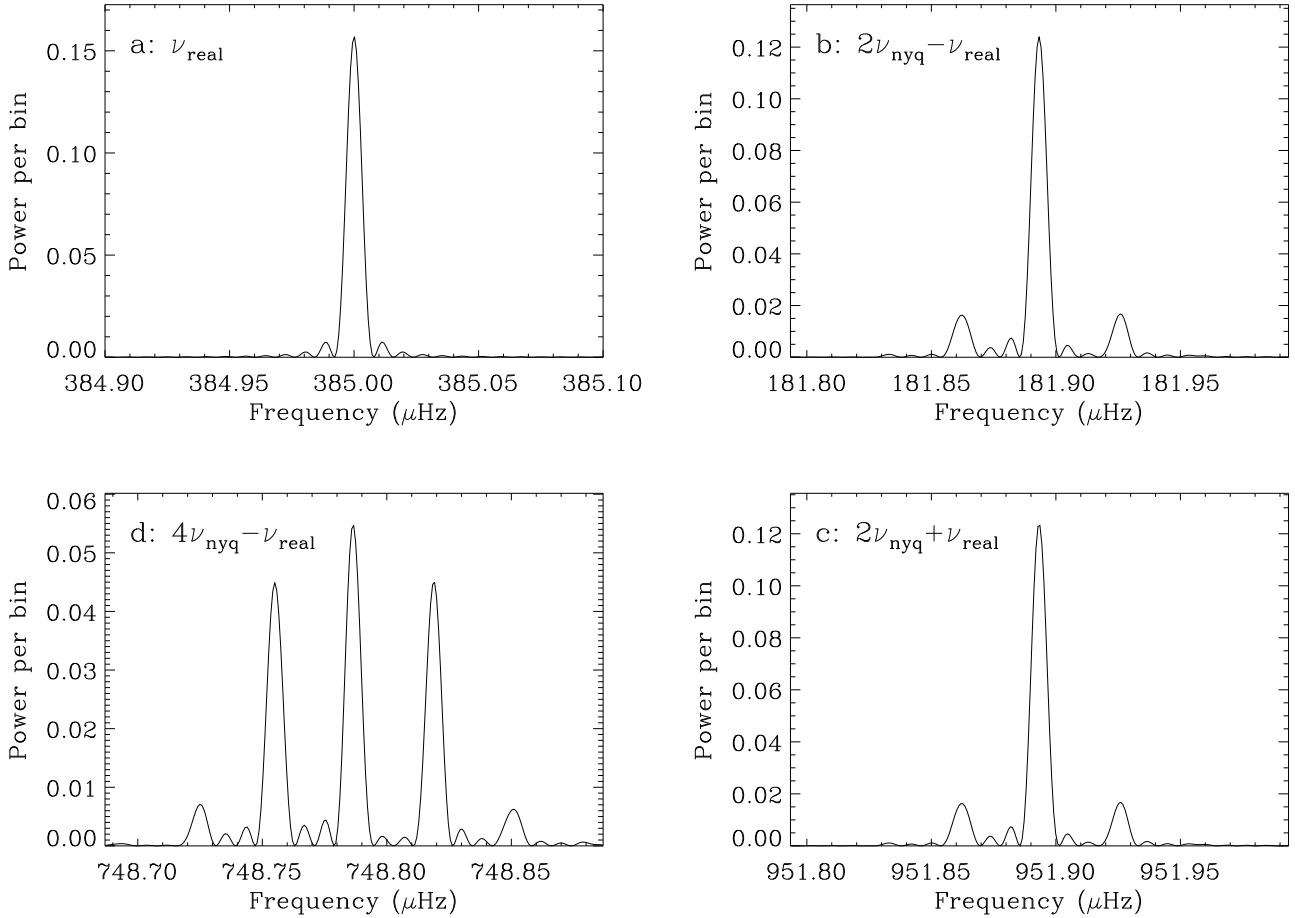


Figure 2. Top left-hand panel: zoom of the peak due to the true frequency marked ‘a’ on the right-hand panel Fig. 1. Other panels: zooms of the aliases marked ‘b’, ‘c’ and ‘d’ on Fig. 1.

(0.05 μHz ; dotted line), 184 days (0.02 μHz ; dark solid line) and 1 yr (0.01 μHz ; grey solid line).

Lifetimes of solar-like oscillations in main-sequence and sub-giant stars are typically of the order of several days in length. The lifetimes of detected radial mode oscillations in red giants can be as long as the 73-day lifetime considered above (e.g., Corsaro et al. 2012). The corresponding dashed line in Fig. 3 would be barely indistinguishable from a Lorentzian profile in the presence of real noise. The same would of course be true for shorter mode lifetimes. The longer lifetimes modelled in Fig. 3 show much more significant departures from a Lorentzian appearance. Provided S/N levels in the observed modes are sufficiently high, it might therefore be possible to discriminate visually the sidebands of some long-lived modes. It is worth noting once more that amplitudes of solar-like oscillations are usually much lower than for coherent pulsators, making it harder to distinguish the sideband structure.

We conclude that an important consequence of the finite mode lifetimes is that in most cases one would no longer be able to distinguish aliased from true oscillation peaks on account of the sideband structure. However, for solar-like oscillators we are fortunate in that we do not need to rely on such discrimination alone.

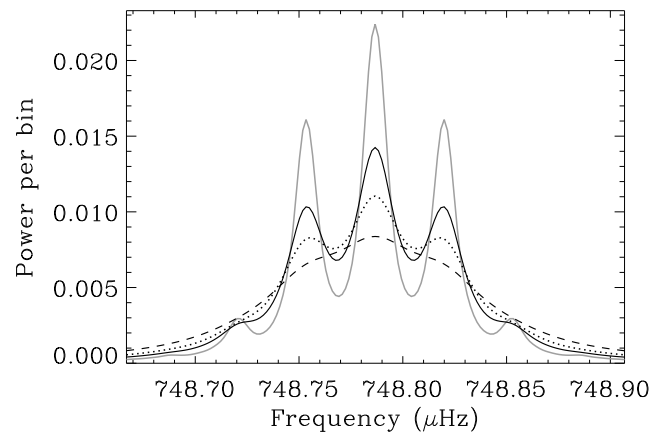


Figure 3. Impact of finite mode lifetimes on the aliased quintuplet from the bottom left-hand panel of Fig. 2. The different linestyles show the composite, aliased profiles expected when the real mode has a lifetime (linewidth) of 73 days (0.1 μHz ; dashed line), 123 days (0.05 μHz ; dotted line), 184 days (0.02 μHz ; dark solid line) and 1 yr (0.01 μHz ; grey solid line).

4.2 Use of a priori information for solar-like oscillators

The rich spectra of overtones shown by solar-like oscillators provides the necessary, a priori information to allow us to select the true spectrum from the aliased spectra. We illustrate how with a real example, the low-luminosity red giant KIC 4351319. This target was observed in both long and short cadence during the nominal *Kepler* Mission. Here, we have used data prepared using the PDC-MAP pipeline (Stumpe et al. 2012; Smith et al. 2012). The top panel of Fig. 4 shows the frequency power spectra of simultaneous LC (upper plot) and SC (lower plot) PDC-MAP data from *Kepler* Quarters Q8 through Q17. The nominal LC Nyquist frequency, ν_{Nyq} , is marked by the vertical dashed line. The luxury afforded by having contemporaneous data available also in SC – where the oscillations are oversampled – of course allows us to tag the peaks in the LC spectrum above ν_{Nyq} as the true oscillation frequencies (see the figure). However, two checks based on use of the LC spectrum alone allow us to make the same call.

The bottom panel of Fig. 4 shows a zoom of the LC spectrum above and below ν_{Nyq} . Our first check relates to the large frequency separation, $\Delta\nu$, the spacing shown by consecutive overtones of the same angular (spherical) degree, l . An extensive body of literature has now established a fairly tight correlation between the average large separation and the observed frequency of maximum oscillation power, ν_{max} (e.g., see Hekker et al. 2009; Stello et al. 2009; Huber et al. 2011; Mosser et al. 2012). This relation may be expressed in the form $\Delta\nu \propto \nu_{\text{max}}^\beta$, with $\beta \approx 0.76$ for the cool subgiants and low-luminosity red giants of interest here. While there is evidently spread in the relation due to, for example, dependences on mass and metallicity, the strong correlation nevertheless allows us to discriminate the true from the aliased spectrum. The lengths of the horizontal arrows in the bottom panel correspond to expected average separations, assuming a ν_{max} of $\approx 190 \mu\text{Hz}$ (peaks below ν_{Nyq}) and $\approx 380 \mu\text{Hz}$ (peaks above ν_{Nyq}). The shaded regions mark the locations of pairs of adjacent $l = 2$ and $l = 0$ modes. The frequency intervals between these regions provide a visual estimate of the observed large separation. Evidently, it is the spectrum above ν_{Nyq} that conforms with the expected average separation.

The second check relates to the relative power shown by adjacent $l = 2$ and $l = 0$ modes. Within each pair, the $l = 0$ mode lies at higher frequency. We expect to see more power in the $l = 0$ mode than in its $l = 2$ counterpart. Whilst predictions of the exact power ratios are rendered uncertain by the complexities of non-adiabatic calculations, observed ratios are usually not too far from the ≈ 2 -to-1 ratio expected from the assumption of energy equipartition and geometric cancellation of the perturbations on the visible stellar disc (when projected on to spherical harmonic functions, with an appropriate limb-darkening law; e.g., see Aerts et al. 2009). Unless the star is observed with the rotation axis along the line-of-sight, power shown by the $l = 2$ modes will be spread across several components (e.g., Gizon & Solanki 2003). The ratio in total power then tends to be exaggerated in the frequency power spectrum because it is the *maximum* power spectral densities, i.e., the heights of the mode peaks, that are immediately apparent from a visual inspection.

Inspection of the mode pairs in the bottom panel of Fig. 3 again implies that the spectrum above ν_{Nyq} is the true one: The $l = 0$ modes, the higher-frequency modes in each marked pair, have the higher observed powers.

4.3 Impact of signal attenuation and background aliasing

How far above ν_{Nyq} might we hope to detect solar-like oscillations in the LC *Kepler* data? A combination of several factors means that pushing the limit well above ν_{Nyq} is challenging. First, the sinc-function attenuation due to the finite integration time leads to significant reduction of the observed oscillation amplitudes at frequencies above ν_{Nyq} . Second, the impact of the sinc attenuation is exacerbated by the fact that the intrinsic maximum amplitudes of solar-like oscillations decrease with increasing ν_{max} . And third, we must also contend with background power aliased from the region below ν_{Nyq} , which has contributions from stellar granulation, stellar activity, shot and instrumental noise. Note that any non-white or “red” noise component, such as the granulation, will also have a contribution above ν_{Nyq} that is sinc-function attenuated, just like the oscillations (e.g., see Kallinger et al. 2014).

We come back to the example of KIC 4351319 to help illustrate these points. The top panel of Fig. 4 shows clearly the attenuated power of the oscillations in the LC spectrum of KIC 4351319, relative to those observed in the SC spectrum. The impact of the sinc-function attenuation on the observed S/N is compounded in the LC spectrum because the background in the region of ν_{max} is the aliased background from lower frequencies, which is dominated by granulation *and* is much higher – by more than an order of magnitude – than the shot-noise background. The spectrum of the oscillations is in reality coincident in frequency with the lower-power, higher-frequency part of the granulation spectrum, as shown by the SC spectrum of KIC 4351319. A much higher S/N is therefore observed in the oscillations when using SC data, because we do not have to contend with aliasing of power from the lower-frequency, higher-power part of the granulation spectrum. Our tests indicate that it is only when K_p is fainter than approximately 11 to 12 mag that the photon shot noise becomes an important factor in determining the detectability of the modes in the LC super-Nyquist regime.

From the observed SC spectrum of KIC 4351319 we may construct an (almost) accurate prediction of the LC spectrum. We begin by multiplying the observed SC spectrum³ by the sinc-squared attenuation filter, η^2 . (Note we have not bothered to attempt to discriminate the white contribution due to shot noise, since it is very small compared to the other contributions.) The predicted LC power below ν_{Nyq} is given by adding the sub-Nyquist SC attenuated power to the aliased, super-Nyquist attenuated spectrum from above ν_{Nyq} (after reflecting the latter about ν_{Nyq}). The predicted LC power above ν_{Nyq} is then just the reflected prediction from below ν_{Nyq} . Fig. 5 shows the resulting prediction (lower plot), together with the LC spectrum from Fig. 4 (upper plot).

When the oscillations are undersampled, the appearance of the oscillations spectra in the super-Nyquist regime depends critically on the proximity of ν_{max} to the boundary at $2\nu_{\text{Nyq}}$. This boundary is where the first zero of the sinc-function attenuation lies, and is also where aliased background power – from granulation, activity and instrumental noise – is most severe, coming as it does from the very low-frequency part of the spectrum. Fig. 6 is an idealized, visual guide to the changing appearance of spectra as ν_{max} is varied. The figure shows schematic frequency-power spectra made by applying suitable scaling relations (see below) to the properties of a sequence of $1 M_\odot$ stellar evolutionary models computed by the Padova group (Marigo et al. 2008). The top left-hand panel of Fig. 6 plots tracks

³ The signatures of the oscillations and granulation are also attenuated in the SC data, but since the SC Nyquist frequency is $\approx 8496 \mu\text{Hz}$ the impact in the frequency range of interest here is negligible.

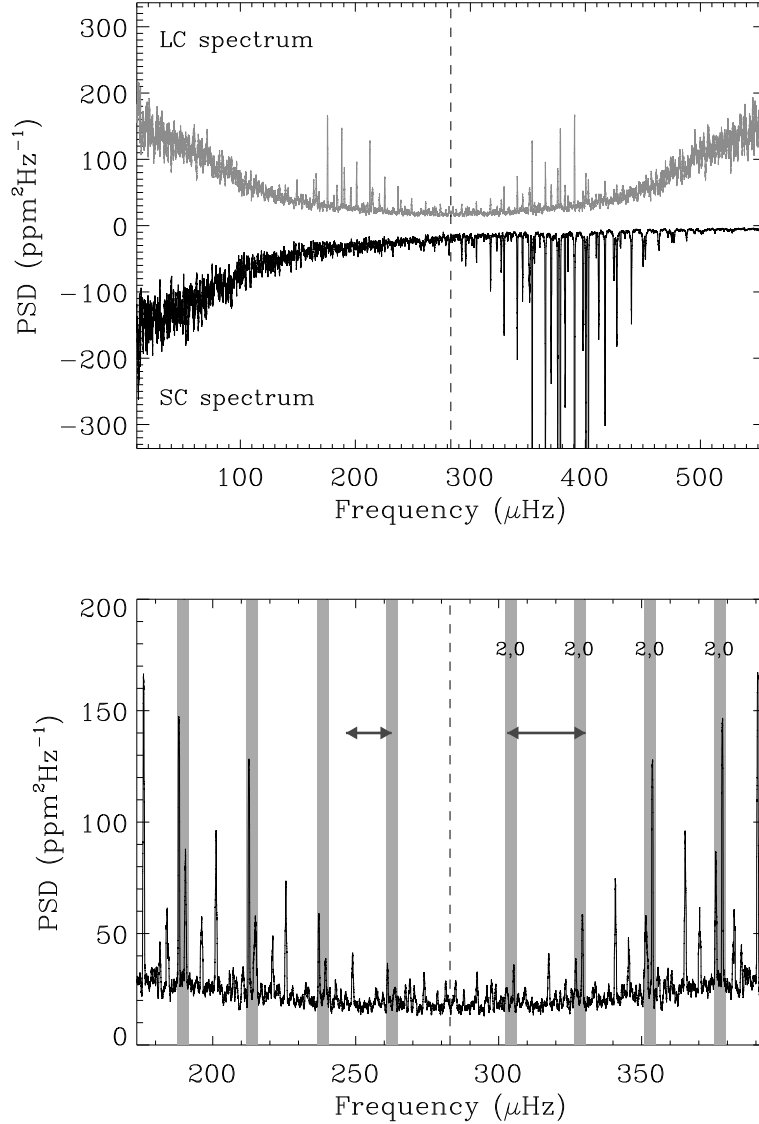


Figure 4. Top panel: frequency power spectra of simultaneous LC (upper plot) and SC (lower plot) data collected by *Kepler* on the low-luminosity red-giant KIC4351319. Bottom panel: zoom of the LC spectrum above and below ν_{Nyq} . The lengths of the horizontal arrows in the bottom panel correspond to expected average separations, assuming a ν_{max} of $\approx 190 \mu\text{Hz}$ (peaks below ν_{Nyq}) and $\approx 380 \mu\text{Hz}$ (peaks above ν_{Nyq}). The shaded regions mark the locations of pairs of adjacent $l = 2$ and $l = 0$ modes.

in the $\log g$ - T_{eff} plane, with the selected models shown in red. All five models have a predicted frequency of maximum solar-like oscillations power, ν_{max} , that lies above ν_{Nyq} . The characteristic ν_{max} frequency was estimated from the fundamental stellar properties (Brown et al. 1991; Kjeldsen & Bedding 1995) using:

$$\nu_{\text{max}} = \nu_{\text{max},\odot} \left(\frac{M}{M_{\odot}} \right) \left(\frac{R}{R_{\odot}} \right)^{-2} \left(\frac{T_{\text{eff}}}{T_{\text{eff},\odot}} \right)^{-0.5}, \quad (4)$$

where we have scaled against the solar values of $\nu_{\text{max},\odot} = 3090 \mu\text{Hz}$ and $T_{\text{eff},\odot} = 5777 \text{ K}$. Loci of constant ν_{Nyq} , and selected multiples thereof, are also marked in the top panel.

After the top left-hand panel of Fig. 6, the other panels show schematic representations of the limit (noise-free) power density spectra expected for LC (upper plots) and SC (lower plots) data, where we assumed each model was observed as a bright *Kepler*

target having a *Kepler* apparent magnitude of $K_p = 9$. The composite SC spectra were constructed using the scaling relations and formulae in Chaplin et al. (2011b), with contributions from oscillations, granulation and shot noise included. We refer the reader to that paper for further details.

There was one ingredient missing from Chaplin et al. (2011b) that we needed to make the spectra, and that was the step to convert estimates of the maximum mode amplitudes, A_{max} , into maximum mode power spectral densities (peak heights) H_{max} . In this paper we have used an appropriate formalism from Chaplin et al. (2008), i.e.,

$$H_{\text{max}} = \frac{2A_{\text{max}}^2}{\pi T \Gamma + 2}, \quad (5)$$

with mode peak linewidths Γ estimated from Appourchaux et al.

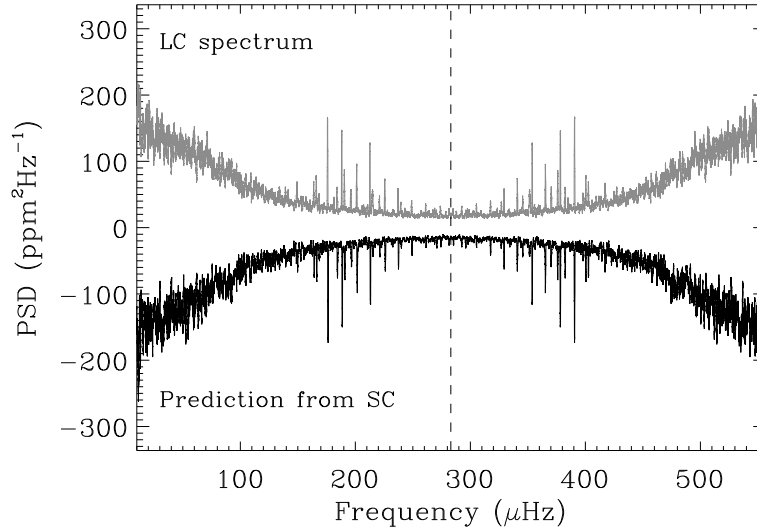


Figure 5. Frequency power-spectrum of KIC 4351319: Upper plot shows LC spectrum, lower plot predicted LC spectrum made from the available SC spectrum.

(2012) using the effective temperature T_{eff} of the models. To avoid cluttering the plots we only mark the predicted limit (noise-free) heights of the radial ($l = 0$) modes; we do not plot the Lorentzian limit profiles or predictions for non-radial modes. The predicted oscillation lifetimes (Lorentzian peak linewidths) are in all cases short (large) enough that the timing sidebands would be unresolved (see Section 4.1), and so each range of ν_{Nyq} would essentially be a near identical, reflected copy.

The predicted SC spectra in Fig. 6 show where the true frequencies lie. Regarding the general appearance of the SC spectra: The power in, and the characteristic timescale of, the granulation both increase with decreasing ν_{max} ; we also recall that the power in the oscillations increases with decreasing ν_{max} . The nature of these changes is such that all composite SC spectra are, in their gross properties at least, approximately homologously scaled versions of one another.

The SC spectra were converted to predicted LC spectra by applying the sinc-squared attenuation in power, followed by suitable aliasing about the ν_{Nyq} boundaries (see Section 4.2). The schematic spectra have been plotted up to a frequency of just over $3\nu_{\text{Nyq}}$, to fully encompass the SC oscillation spectrum of the highest ν_{max} (least evolved) stellar model. The vertical dashed lines mark the ν_{Nyq} boundaries. Frequency aliasing adds to the complexity of the LC spectra, more severely in some cases than others depending on the placement of the true frequencies with respect to the multiple ν_{Nyq} boundaries. These plots show very clearly how attenuation of the oscillations can have a drastic impact on the observed S/N when the true frequencies are undersampled and hence lie in the super-Nyquist regime. The oscillation peaks are barely observable in the highest ν_{max} case shown here.

Before summarizing results from our simulations, it is worth noting that we have not included any low-frequency contributions due to stellar activity or instrumental or data-reduction noise. The predicted S/N ratios implied by the modelled spectra should therefore be regarded as upper-limit estimates. Nevertheless, starting from the detection recipe in Chaplin et al. (2011b), we have estimated detection probabilities for each of these modelled cases. We folded in predicted power from the non-radial modes, and modi-

fied the detection algorithm to operate on the composite, aliased spectrum in a single range of ν_{Nyq} . Our predictions suggest that for the targets in the nominal-Mission *Kepler* archive with 4 yr of data, the upper limit for detections will be around $\nu_{\text{max}} \approx 500 \mu\text{Hz}$. Instrumental noise levels will be higher for K2 (Howell et al. 2014), however, with reference to the above, intrinsic stellar noise should remain the limiting factor for brighter targets. Taking $T = 75$ days, the length of each K2 campaign, we estimate an absolute upper detection limit between $\nu_{\text{max}} \approx 400$ and $\approx 450 \mu\text{Hz}$.

4.4 Some real examples

Fig. 7 shows some more super-Nyquist examples from the *Kepler* archive. Five targets with *Kepler* LC and SC data have been selected that have undersampled oscillations in LC. The ν_{max} values range from $\approx 320 \mu\text{Hz}$ (just above ν_{Nyq}) to $\approx 550 \mu\text{Hz}$ (just below $2\nu_{\text{Nyq}}$). It is worth stressing that there are not many targets like this in the *Kepler* archive with SC data (in particular at the low end of the range). The top left-hand panel plots the locations of the stars in the $\log g$ - T_{eff} plane, with stellar properties taken from Chaplin et al. (2014). The main plots of the other panels show zooms of the LC power spectra in the undersampled, super-Nyquist regions where the real oscillation frequencies lie. Note that we chose a slightly different layout compared to the previous figures to show more clearly the lower S/N cases at higher ν_{max} . The insets show power spectra computed from available SC data. Note that, unlike KIC 4351319, the SC coverage was much more limited for some of these stars. Even though the SC and LC data are not necessarily contemporaneous, the insets show clearly where the real oscillations are.

From our model predictions above, we expect to have good sensitivity up to $\nu_{\text{max}} \approx 400 \mu\text{Hz}$, a conclusion that is borne out by these real data. At frequencies above this, detecting the modes becomes more difficult. Signatures of the oscillations are clearly apparent in the LC spectrum of KIC 6531928 ($\nu_{\text{max}} \approx 450 \mu\text{Hz}$) but at a much reduced S/N compared to the other targets. KIC 8038445 has a ν_{max} of $490 \mu\text{Hz}$. Signatures of a few modes are just detectable in its LC spectrum. This case marks the approximate upper ν_{max} limit for making detections in the archival *Kepler* data.

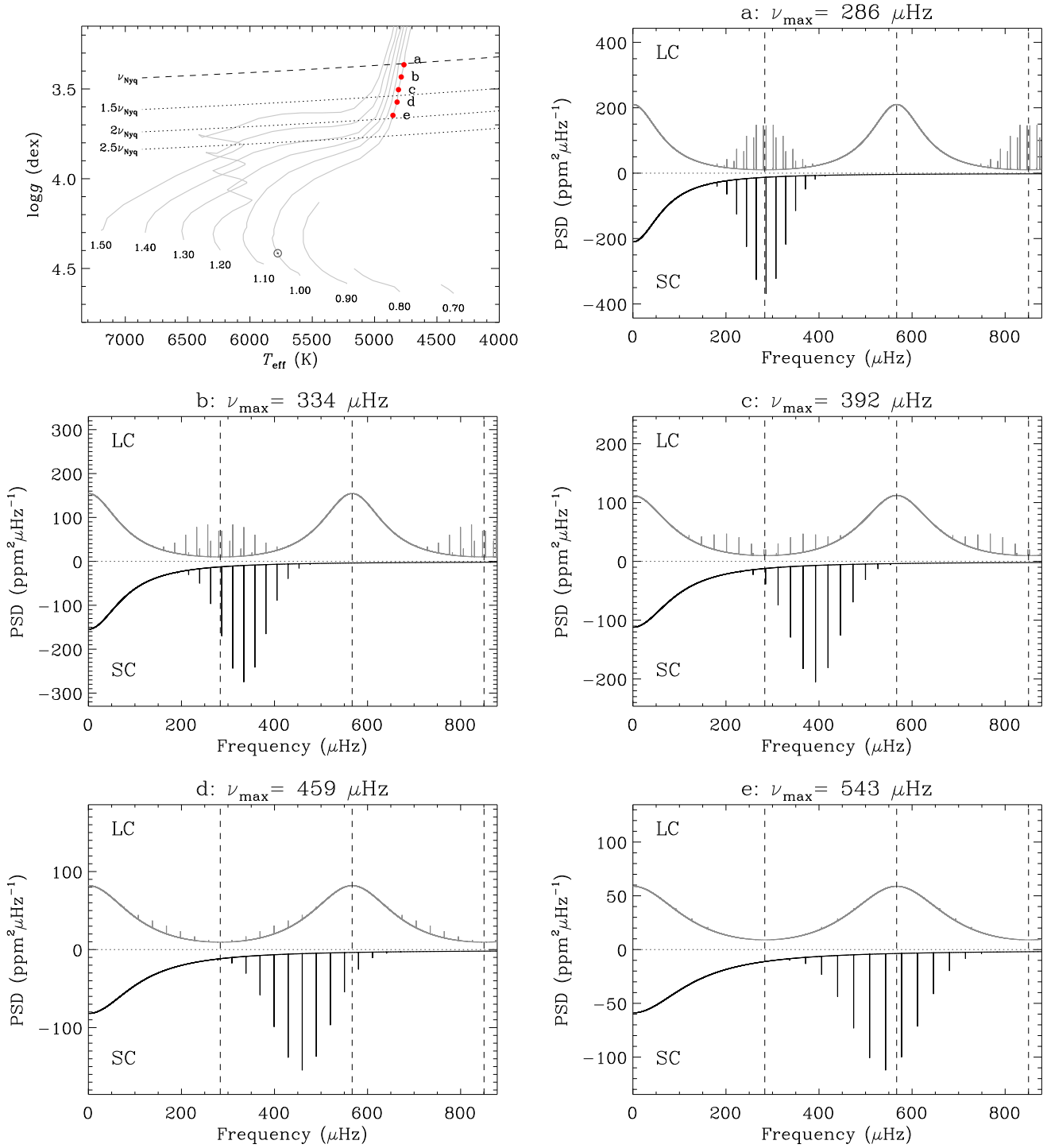


Figure 6. Idealized guide to the changing appearance of undersampled and oversampled oscillations spectra with varying ν_{\max} , based on predictions using scaling relations applied to the fundamental properties of several $1 M_{\odot}$ stellar models. The top left-hand panel shows the locations of the models in the $\log g - T_{\text{eff}}$ plane. The other panels show schematic representations of the limit (noise-free) power density spectra expected for LC (undersampled, upper plots) and SC (oversampled, lower plots) data, assuming each model was observed as a bright *Kepler* target having a *Kepler* apparent magnitude of $K_p = 9$. Spectra are plotted up to a frequency of just over $3\nu_{\text{Nyq}}$ – with dashed lines marking ν_{Nyq} boundaries – to fully include the SC oscillation spectrum of the highest ν_{\max} (least evolved) stellar model (see plot titles).

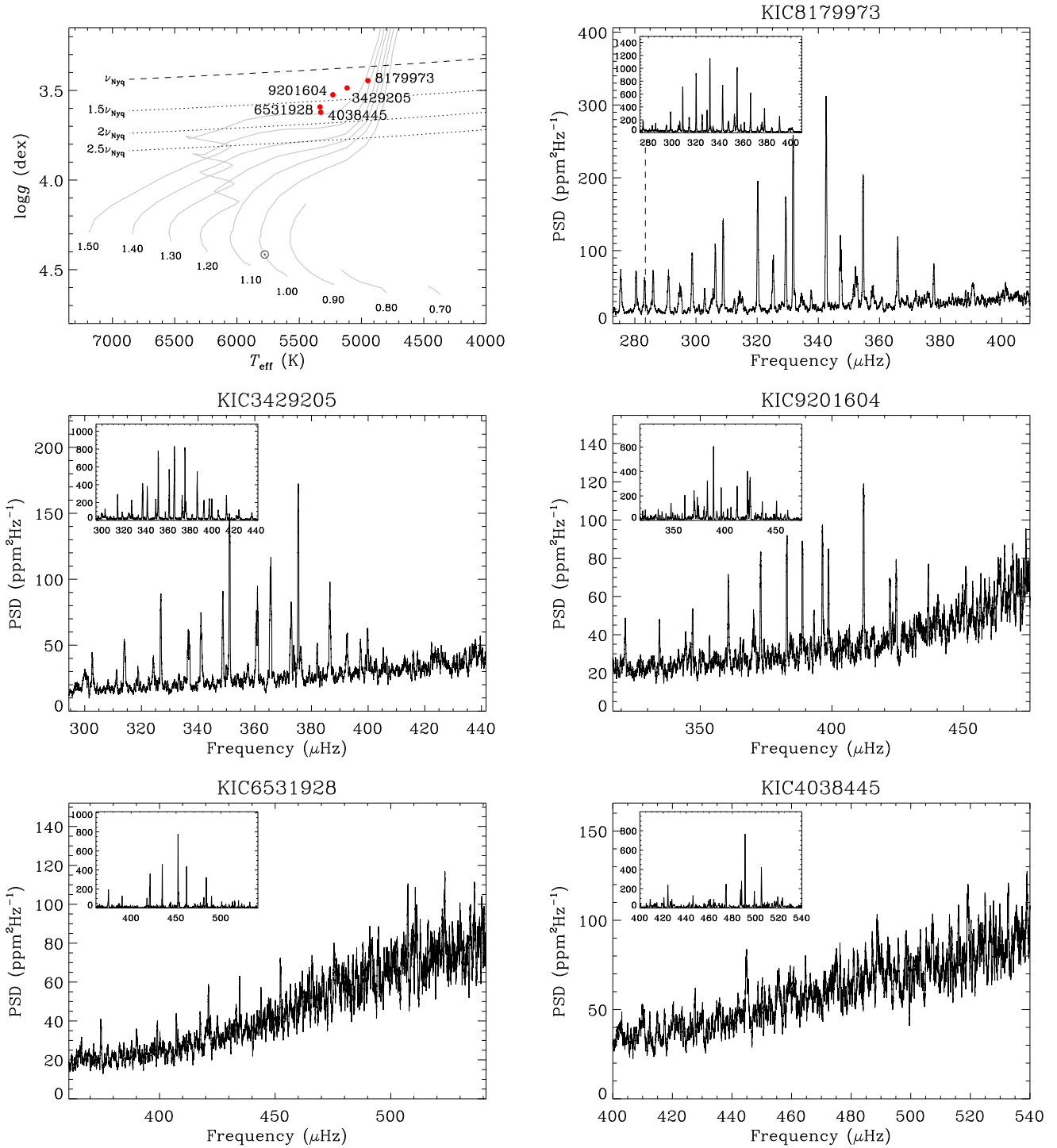


Figure 7. Demonstration, using real *Kepler* LC data on five stars, of undersampled solar-like oscillation spectra in the LC super-Nyquist regime. Each target also has some SC data available, in which the oscillations are oversampled. The top left-hand panel shows the locations of the stars in the $\log g$ - T_{eff} plane. Other panels: main plots show the LC power spectra (oscillations undersampled), insets show power spectra computed from available SC data (oscillations oversampled).

Things become much more challenging as we move to higher frequencies, to the region where ν_{max} straddles or lies close to the boundary at $2\nu_{\text{Nyq}}$. Imposing a high-pass filter to suppress the very-low frequency background power in the sub-Nyquist regime does not help to improve the S/N in the super-Nyquist regime: the filter-

ing response is the same in each domain of ν_{Nyq} and so any oscillation signal is also filtered.

5 CONCLUSION

We have considered the prospects for detecting solar-like oscillations in the undersampled “super-Nyquist” regime of long-cadence (LC) *Kepler* data, i.e., above the LC Nyquist frequency of $\approx 283 \mu\text{Hz}$. We conclude that the LC data may be utilized for asteroseismic studies of targets whose dominant oscillation frequencies lie as high as $\approx 500 \mu\text{Hz}$. The frequency detection threshold for the shorter-duration K2 science campaigns is lower. We estimate that the robust threshold will lie somewhere between ≈ 400 and $450 \mu\text{Hz}$.

These stars would usually be studied with *Kepler* short-cadence (SC) data. The oscillations are then oversampled, since the associated Nyquist frequency of $\approx 8496 \mu\text{Hz}$ lies well above the frequencies of the detectable oscillations. However, the number of SC available target slots is very limited: indeed, there are around only 50 targets of interest in the *Kepler* archive that have detected oscillations in SC data and v_{max} between the LC ν_{Nyq} and $\approx 500 \mu\text{Hz}$. In most of these cases there is only 1 month of data from the initial asteroseismic survey phase. This precludes very detailed studies of these targets, which demands high-frequency-resolution datasets for analyses of individual modes (including rotational frequency splittings).

The exploitation of the archival *Kepler* and new K2 data for LC super-Nyquist studies offers the prospect of increasing significantly the number of evolved subgiant and low-luminosity red-giant targets available for asteroseismic study. By making use of the revised catalogue of *Kepler* star properties in Huber et al. (2014), we estimate that up to 400 targets may be available for study in the *Kepler* archive. Moreover, many of these targets will have data spanning the entire nominal Mission, giving the frequency resolution needed for the abovementioned analyses of individual modes.

The potential number of targets amenable to study with K2 data could run into the thousands, since new target lists will be generated for each campaign.

ACKNOWLEDGEMENTS

Funding for this Discovery mission is provided by NASA’s Science Mission Directorate. The authors wish to thank the entire *Kepler* team, without whom these results would not be possible. W.J.C., Y.E., G.R.D., T.L.C., R.H. and A.M acknowledge the support of the UK Science and Technology Facilities Council (STFC). Funding for the Stellar Astrophysics Centre is provided by The Danish National Research Foundation (Grant agreement no.: DNR106). The research leading to these results has received funding from the European Community’s Seventh Framework Programme ([FP7/2007-2013]) under grant agreement no. 312844 (SPACEINN).

REFERENCES

Aerts, C., Christensen-Dalsgaard, J., Kurtz, D. W., 2009, *Asteroseismology*, Springer Science
 Appourchaux, T., Benomar, O., Gruberbauer, M., et al., 2012, *A&A*, 537, 134
 Baran, A. S., Reed, M. D., Stello, D., et al., 2012, *MNRAS*, 424, 2686
 Beck, P. G., Hambleton, K., Vos, J., et al., 2014, *A&A*, 564, 36
 Brown, T. M., Gilliland, R. L., Noyes, R. W., Ramsey, L. W., 1991, *ApJ*, 368, 599

Campante, T. L., 2012, PhD thesis, Universidade do Porto (arXiv:1405.3145)
 Chaplin, W. J., Miglio, A., 2013, *ARA&A*, 51, 353
 Chaplin, W. J., Elsworth, Y., Isaak, G. R., Miller, B. A., New, R., 2002, *MNRAS*, 330, 731
 Chaplin, W. J., Houdek, G., Appourchaux, T., et al. 2008, *A&A*, 485, 813
 Chaplin, W. J., Kjeldsen, H., Christensen-Dalsgaard, J., et al., 2011a, *Science*, 332, 213
 Chaplin, W. J., Kjeldsen, H., Bedding, T. R., et al., 2011b, *ApJ*, 732, 54
 Chaplin, W. J., Kjeldsen, H., Christensen-Dalsgaard, J., et al., 2013, *Kepler White Paper* (arXiv:1309.0702)
 Chaplin, W. J., Basu, S., Huber, D., et al., 2014, *ApJS*, 210, 1
 Corsaro, E., Stello, D., Huber, D., Bedding, T. R., et al., 2012, *ApJ*, 757, 190
 Davies, G. R., Miglio, A., Handberg, R., Campante, T. L., Chaplin, W. J., Elsworth, Y., 2014, *ApJ*, in the press (arXiv:1408.7042)
 Dupret, M.-A., Belkacem, K., Samadi, R., et al., 2009, *A&A*, 506, 57
 García, R. A., Mathur, S., Pires, S., et al., 2014, *A&A*, 568, A10
 Gaulme, P., McKeever, J., Rawls, M. L., Jackiewicz, J., Mosser, B., Guzik, J. A., 2013, *ApJ*, 767, 82
 Gilliland, R. L., Brown, T. M., Christensen-Dalsgaard, J., et al., 2010, *PASP*, 122, 131
 Gilliland, R. L., Chaplin, W. J., Dunham, E. W., et al., 2011, *ApJS*, 197, 6
 Gizon, L., Solanki, S. K., 2003, *ApJ*, 589, 1009
 Hekker, S., Kallinger, T., Baudin, F., et al., 2009, *A&A*, 506, 465
 Hekker, S., Gilliland, R. L., Elsworth, Y., et al., 2011, *MNRAS*, 411, 2594
 Hermes, J. J., Charpinet, S., Barclay, T., et al., 2014, *ApJ*, 789, 85
 Howell, S. B., Sobeck, C., Haas, M., et al., 2014, *PASP*, 126, 398
 Huber, D., Bedding, T. R., Stello, D., et al., 2011, *ApJ*, 743, 143
 Huber, D., Chaplin, W. J., Christensen-Dalsgaard, J., et al., 2013, *ApJ*, 767, 127
 Huber, D., Silva Aguirre, V., Matthews, J. M., et al., 2014, *ApJS*, 211, 2
 Jeffery, C. S., Ramsay, G., 2014, *MNRAS*, 442, L61
 Jenkins, J. M., Caldwell, D. A., Chandrasekaran, H., et al., 2010, *ApJ*, 713L, 120
 Kallinger, T., De Ridder, J., Hekker, S., et al., 2014, *A&A*, in press (arXiv:1408.0817)
 Kjeldsen, H., Bedding, T. R., 1995, *A&A*, 293, 87
 Koch, D. G., Borucki, W. J., Rowe, J. F., et al., 2010, *ApJ*, 713, L131
 Marigo, P., Girardi, L., Bressan, A., et al. 2008, *A&A*, 482, 883
 Mosser, B., Elsworth, Y., Hekker, S., et al., 2012, *A&A*, 537, 30
 Murphy, S. J., 2012, *MNRAS*, 422, 665
 Murphy, S. J., Shibahashi, H., Kurtz, D. W., 2013, *MNRAS*, 430, 2986
 Nyquist, H., 1928, *Transactions of the American Institute of Electrical Engineers*, 47, 617
 Shannon, C. E., 1949, *Proceedings of the Institute of Radio Engineers*, 37, 10
 Smith, J. C., Stumpe, C., Van Cleve, J. E., et al. 2012, *PASP*, 124, 1000
 Stello, D., Chaplin, W. J., Basu, S., et al., 2009, *MNRAS*, 400, 80L
 Stello, D., Huber, D., Bedding, T. R., et al., 2013, *ApJ*, 765, L41
 Stumpe, M. C., Smith, J. C., Van Cleve, J. E., et al. 2012, *PASP*, 124, 985